

Tidal Capture of Stars by Intermediate-Mass Black Holes

H. Baumgardt^{1*}, C. Hopman^{2*}, S. Portegies Zwart^{3,4*} and J. Makino^{5*}

¹*Sternwarte, University of Bonn, Auf dem Hügel 71, 53121 Bonn, Germany*

²*Faculty of Physics, Weizmann Institute of Science, P.O. Box 26, Rehovot 76100, Israel*

³*Astronomical Institute “Anton Pannekoek,” University of Amsterdam, Kruislaan 403, Netherlands*

⁴*Section Computational Science, University of Amsterdam, Kruislaan 403, Netherlands*

⁵*Department of Astronomy, University of Tokyo, 7-3-1 Hongo, Bunkyo-ku, Tokyo 113-0033, Japan*

Accepted ????. Received ?????; in original form ?????

ABSTRACT

Recent X-ray observations and theoretical modelling have made it plausible that some ultraluminous X-ray sources (ULX) are powered by intermediate-mass black holes (IMBHs). N-body simulations have also shown that runaway merging of stars in dense star clusters is a way to form IMBHs. In the present paper we have performed N -body simulations of young clusters such as MGG-11 of M82 in which IMBHs form through runaway merging. We took into account the effect of tidal heating of stars by the IMBH to study the tidal capture and disruption of stars by IMBHs. Our results show that the IMBHs have a high chance of capturing stars through tidal heating within a few core relaxation times and we find that 1/3 of all runs contain a ULX within the age limits of MGG-11, a result consistent with the fact that a ULX is found in this galaxy. Our results strengthen the case for some ULX being powered by intermediate-mass black holes.

Key words: globular clusters: general – black hole physics – stellar dynamics

1 INTRODUCTION

Ultra-luminous X-ray sources (ULX) are point-like X-ray sources with isotropic X-ray luminosities in excess of $L = 10^{40}$ erg/sec. Various theories have been proposed in the literature concerning the nature of ULX, like stellar-mass black hole binaries with mild geometrical beaming (King et al. 2001, Rappaport, Podsiadlowski & Pfahl 2005) or high-redshift quasars (Gutiérrez & López-Corredoira 2005) and it is likely that ULX are not a homogeneous class of objects (Soria, Cropper & Motch 2001). Although luminous X-ray sources have been observed in different kinds of environments, sources with luminosities of $L \approx 2 \cdot 10^{39}$ erg/sec or brighter seem to be associated with young stellar populations of star-forming galaxies (Irwin, Bregman & Athey 2004; Swartz et al. 2004).

Since the Eddington luminosity of a star of mass M is given by

$$L_{\text{Edd}} = 1.3 \times 10^{38} \text{ ergs}^{-1} \frac{M}{M_{\odot}} \quad (1)$$

where M is the mass of the accreting object, most low-luminosity ULX are probably stellar-mass black holes. However, there is mounting evidence that the brightest ULX

with luminosities exceeding $L > 10^{40}$ erg s⁻¹ could be intermediate-mass black holes (IMBHs, see Miller & Colbert 2004 for a review). The starburst galaxy M82 for example hosts a ULX with brightness in the range $L = (0.5 - 1.6) \cdot 10^{41}$ ergs⁻¹ (Matsumoto et al. 2001, Kaaret et al. 2001), corresponding to a black hole with mass 350 – 1200 M_{\odot} if emitting photons at the Eddington luminosity. The case for an IMBH in M82 is supported by a 54mHz quasi-periodic oscillation found in the X-ray flux (Strohmayer & Mushotzky 2003) and also by the soft X-ray spectrum of this source (Fiorito & Titarchuk 2004). Another argument supporting the connection between ULX and IMBHs are cool thermal emission components which have been found in the X-ray spectra of some ULX and which can be fitted well with accretion disc models of IMBHs (Miller, Fabian & Miller 2004).

Portegies Zwart et al. (2004) have performed N -body simulations of the dense star cluster MGG-11 whose position coincides with the ULX in M82. They found that runaway merging of massive main-sequence stars in the centre of this cluster leads to the formation of a massive star with a mass of several 1000 M_{\odot} within a few Myrs if the initial concentration of the cluster is larger than that of a King $W_0 = 9.0$ model. The connection between an IMBH and the ULX was strengthened by Hopman, Portegies Zwart & Alexander (2004) who showed through analytic estimates that an IMBH with a mass of 1000 M_{\odot} residing in the centre of MGG-11 has a high probability of tidally capturing a

* e-mail: holger@astro.uni-bonn.de (HB); clovis.hopman@weizmann.ac.il (CH); spz@science.uva.nl (SPZ); makino@astron.s.u-tokyo.ac.jp (JM)

passing main-sequence star or giant. The orbit of the captured star was found to circularise even when dynamical perturbations by other cluster stars were taken into account and the system entered a Roche-lobe overflow (RLOF) phase once the captured star had sufficiently increased its radius through stellar evolution.

Portegies Zwart, Dewi & MacCarone (2004) and Li (2004) showed that IMBHs with mass-transferring companions near the end of their main-sequence lifetimes are able to create X-ray luminosities in excess of $L = 10^{40} \text{ergs}^{-1}$ over several Myrs, giving them a high chance to be observed as ULX. For sufficiently low-mass companions, the RLOF mass transfer stage might start after the host cluster has been dissolved by the tidal field of the parent galaxy, offering a way to explain isolated ULX (Hopman, Portegies Zwart & Alexander 2004).

In this paper we present the results of detailed N -body simulations of the formation and further evolution of an IMBH in a cluster with characteristics similar to MGG-11 in the starburst Galaxy M82 (see Portegies Zwart et al. 2004). Our simulations included the effects of tidal heating and the emission of gravitational waves of passing stars and we investigated the chances that MGG-11 produces a ULX within the age limits determined by observations (7-12 Myrs).

This paper is organised as follows: In section 2 we review the theory of tidal heating and section 3 gives analytic estimates of tidal inspiral. Section 4 describes the implementation of tidal heating into our simulations. Section 5 discusses our results for MGG-11 and section 6 summarises the paper and presents our conclusions.

2 TIDAL HEATING OF STARS NEAR A MASSIVE BLACK HOLE

Stellar systems are usually well described as a system of point particles interacting with Newtonian gravity. In a few cases, however, when the stellar density is sufficiently high, this approximation is no longer accurate and fails to describe some of the important processes which occur in stellar clusters. General relativistic effects for example become important when stars approach each other at distances close to their Schwarzschild radius, which can be relevant for compact stars. Main sequence stars are much larger and close encounters can lead to hydrodynamical interactions, with stellar collisions as the extreme. This may lead to a runaway merger in young and dense star clusters (Portegies Zwart et al. 1999; Portegies Zwart & McMillan 2002; Freitag, Gürkan & Rasio 2005; see also section 5).

Stars that pass each other at somewhat larger distances may still affect each others orbits by energy dissipation in a tidal interaction. Such an interaction may initiate tidal modes on both stars. The energy invested to raise the tides in the stars is taken from their kinetic energies (Press & Teukolsky 1977). Two initially unbound stars may so become bound, or a bound eccentric binary can become bound more tightly.

Stars can also have a tidal interaction with a black hole (BH). The length-scale for tidal forces of an IMBH of mass M_\bullet on a star of mass M_\star and radius R_\star to become important

is given by the tidal radius (see e.g. Kochanek 1992):

$$r_t \simeq \left(\frac{M_\bullet}{M_\star} \right)^{1/3} R_\star. \quad (2)$$

We now recognise several distinct regimes: (1) The pericenter distance is much larger than the tidal radius ($r_p \gg r_t$), in which case tidal effects are negligible. (2) The distance of closest approach is smaller than the tidal radius $r_p < r_t$. In this case the entire star may be disrupted or part of its envelope may be stripped off to form a temporary accretion disk around the black hole. The gas accreting from the star or the disc onto the black hole then causes a flare. The duration of the flare depends on how violent the interaction was and whether or not an accretion disc was formed: for tidal disruptions around super-massive black holes the flare might last at most a few years (Rees 1988). (3) In the intermediate regime ($r_p \gtrsim r_t$), the star is tidally deformed, and orbital kinetic energy is transferred to the internal energy of the star. We call this the tidal capture regime.

For highly eccentric orbits ($e \gtrsim 0.9$), the energy dissipation per orbit can be parametrised by

$$\Delta E_t = \frac{GM_\star^2}{R_\star} \left(\frac{M_\bullet}{M_\star} \right)^2 \sum_{l=2}^{\infty} \left(\frac{R_\star}{r_p} \right)^{2l+2} T_l(\eta), \quad (3)$$

where

$$\eta = \left(\frac{M_\star}{M_\star + M_\bullet} \right)^{1/2} \left(\frac{r_p}{R_\star} \right)^{3/2}. \quad (4)$$

Here $T_l(\eta)$ is the dimensionless tidal coupling function, which depends on the stellar structure and is a strongly decreasing function of the pericenter r_p (see e.g. Press & Teukolsky 1977). The orbital energy at the tidal radius usually exceeds the binding energy of the star by several orders of magnitude, and some fraction of the orbital energy is dissipated at every new pericenter passage. As a result the star becomes very hot and expands. Both effects make it more luminous. The stellar luminosity can become much larger than that achieved by nuclear burning, and is of order

$$L_t = \frac{\Delta E_t}{P}. \quad (5)$$

Here P is the orbital period of the binary system.

It is unclear where a star stores the excess tidal energy. In the two most extreme cases, the star can store the excess energy in the surface layers, or in the bulk of the stellar material. The first case leads to high surface temperatures without appreciable expansion of the star (McMillan, Dermott & Taam 1987), whereas the latter causes the star to remain cold but expand dramatically (Podsiadlowski 1996). Alexander & Morris 2003 dubbed the two possibilities as “hot” and “cold” squeezars and argued that these tidally excited stars may be observable in the center of the Milky-Way Galaxy.

The long-term response of the star to tidal heating determines whether the star survives the encounter. To be able to survive the tidal circularisation near r_t , a star on an initially wide orbit has to dissipate

$$E_t \sim \left(\frac{M_\bullet}{M_\star} \right)^{2/3} \frac{GM_\star^2}{R_\star}, \quad (6)$$

which generally is much larger than the binding energy of the star. As a consequence, a star can only survive a strong

tidal interaction if it cools efficiently. The most obvious way this can be achieved is by radiation, i.e. a “hot squeezer”.

The structure of a “hot squeezer” is unaffected by the encounter, and as a result the cooling of the star is limited by the Eddington luminosity. The limiting luminosity can now be used to compute a lower limit on the pericenter for which the star is able to survive an encounter. The further orbital evolution can be described analytically and the time-scale for complete circularisation of the orbit is then (Alexander & Morris 2003):

$$t_0(r_p, a) = \frac{2\pi M_* \sqrt{GM_* a}}{\Delta E_t(r_p)}. \quad (7)$$

If this time-scale is sufficiently small, the orbit of the star is not changed significantly by scattering with field stars during inspiral (section 3.3). In this case the star circularises near the tidal radius of the IMBH. The subsequent evolution of the IMBH with main-sequence star binary is discussed in section (5.5).

3 ANALYTICAL ESTIMATES OF TIDAL INSPIRAL IN PRESENCE OF SCATTERING

If a star has an orbit in the tidal capture regime ($r_p \gtrsim r_t$) after a first encounter with an IMBH, it experiences repeated tidal interactions through which the orbit shrinks and becomes circularised. The time-scale for circularisation is much larger than the orbital period P of the star ($t_0 \gg P$). If the orbit is perturbed by another star during the inspiral process, the inspiraling star may either be scattered to a wider orbit or into a tighter orbit. In the first case tidal heating will become less effective and the inspiral process slows down or stops completely, making the star more vulnerable for subsequent dynamical interactions. In the latter case the inspiral process is either accelerated or, if the pericenter distance becomes smaller than the tidal radius of the star, the star is tidally disrupted by the IMBH and the inspiral process ends.

3.1 Assumptions

We present an approach which is quite similar for tidal disruptions and tidal inspirals. To obtain analytical estimates for the two processes, we make several assumptions that are generally made for the treatment of tidal disruptions (e.g. Lightman and Shapiro 1977; Frank & Rees 1976; Cohn & Kulsrud 1978; Syer & Ulmer 1999; Magorrian & Tremaine 1999; Miralda-Escudé & Gould 2000; Freitag 2001a; Alexander & Hopman 2003; Wang & Merritt 2004) and inspiral processes (e.g. Hills & Bender 1995; Sigurdsson & Rees 1997; Ivanov 2002; Freitag 2001b, 2003; Alexander & Hopman 2003; Hopman, Portegies Zwart & Alexander 2004; Hopman & Alexander 2005).

Our simple analytical model captures some of the physical mechanisms of the cluster and gives approximately the correct estimates for the probability that a star is captured by the IMBH. Since many of the assumptions listed here have been made by numerous previous papers, it is of importance to trace to what extent the analytical model agrees with the simulations, which has less number of simplifying assumptions.

Here we list our assumptions and discuss them.

(i) The stellar distribution function is well approximated by a stellar cusp, i.e.

$$n_*(r) = \frac{(3 - \alpha)N_a}{4\pi r_a^3} \left(\frac{r}{r_a}\right)^{-\alpha}, \quad (8)$$

where α is approximately constant within the radius of influence r_a of the IMBH (Bahcall & Wolf 1976, 1977), and N_a is the number of stars within r_a .

This assumption is shown to be satisfied by earlier N-body simulations (Baumgardt et al. 2004a; 2004b; Preto, Merritt & Spurzem 2004), and also in our current simulations. The slope of the cusp in our simulations is $\alpha \approx 1.5$. A stellar cusp with $\alpha \approx 1.5$ has also been observed by star counts near the MBH in our Galactic Centre (Alexander 1999). We will assume $\alpha = 3/2$ in the following analysis. This simplifies the expressions somewhat, because in that case the relaxation time is constant (see eq. [12]).

Baumgardt, Makino & Ebisuzaki (2004a) have shown that for small-mass black holes, containing less than a few percent of the total cluster mass, the radius of influence of the black hole is given by

$$r_a = \frac{GM_*}{\sigma_c^2}, \quad (9)$$

where σ is the velocity dispersion in the cluster core.

(ii) Within r_a the orbits of the stars are Keplerian to good approximation. This is a good assumption for our purposes, and it makes many of the expressions more transparent.

(iii) The relaxation time within the cusp is much larger than the orbital time. Stars exchange energy and angular momentum only through small angle two-body interactions.

(iv) Within the radius of influence the stellar population can be approximated by a single mass population.

This assumption is made for simplicity, and much of the discrepancy between the analytical model and the simulations stems from this assumption. In a young stellar cluster there is a wide range of masses, with a few stars which have masses much larger than the mean stellar mass $\langle M_* \rangle$. As a result the most massive stars sink to the IMBH, and the masses within the radius of influence vary strongly. This has considerable consequences for the dynamical behaviour close to the IMBH which the simple analytical model fails to describe. We will comment on this when we discuss the results of our simulations.

(v) Stars reach the IMBH by diffusion of angular momentum rather than energy.

This assumption is accurate for a single mass distribution (Bahcall & Wolf 1976). When a few very massive stars are present in the cluster, however, dynamical friction operates on a time-scale $t_{d.f.} \sim (\langle M_* \rangle / M_*) t_r$, much shorter than the relaxation time t_r . The dynamical mechanism which drives stars to inspiral orbits in a young stellar cluster therefore typically operates in two phases. First there is an “energy phase”, during which a massive star loses energy to field stars and sinks to the centre; this is a purely elastic phase during which there is no tidal heating. Then follows an “angular momentum phase”, during which more interactions with cluster stars change the angular momentum of the massive star, until it finally reaches an orbit with pericenter close

enough to the tidal radius, and tidal heating becomes efficient.

As a result of our simplifying assumptions, the following analysis does not describe the radial distribution function (DF) of the stars as a function of their mass. But once this DF is given, it does provide a treatment of the interplay between scattering and dissipation which is in good agreement with the simulations.

3.2 Tidal disruption

Tidal disruption of stars by an IMBH occurs when a star on an eccentric orbit has angular momentum smaller than the angular momentum at the “loss cone” (J_{lc}). For a main-sequence star orbiting an IMBH, the loss-cone is defined as:

$$J_{lc} = \sqrt{2GM_{\bullet}r_t}. \quad (10)$$

The disruption rate and distribution of stars in angular momentum were studied by Lightman & Shapiro (1977). Here the average changes in momentum are much smaller than J_{lc} (diffusive regime). For this case the time-scale for changes of the pericenter by (small angle) scattering is (Alexander & Hopman 2003)

$$t_p(r_p, a) = \frac{r_p}{a} t_r. \quad (11)$$

Here t_r is the relaxation time, which we can estimate with

$$t_r = A_{\Lambda} \left(\frac{M_{\bullet}}{M_{\star}} \right)^2 \frac{P}{N(< r)} \quad (12)$$

Here A_{Λ} is a constant which includes the Coulomb logarithm, and $N(< r) \propto r^{3-\alpha}$ is the number of stars enclosed within r . For $\alpha = 3/2$ the relaxation time is independent of distance from the IMBH.

The diffusive regime is then defined to be the region where $a < r_{crit}$; r_{crit} is the semi-major axis for which $P(r_{crit}) = t_p(r_t, r_{crit})$,

$$r_{crit} = \left(\frac{1}{2\pi} \sqrt{GM_{\bullet}r_t t_r} \right)^{2/5}. \quad (13)$$

The angular momentum of stars with $a < r_{crit}$ changes by an amount smaller than J_{lc} per orbit, while the change in angular momentum per orbit is larger than J_{lc} if $a > r_{crit}$. In the latter case the velocity distribution can be isotropic, since it is not affected by the presence of the loss-cone. This is not true for the diffusive regime.

The distribution function and merger rate in the diffusive regime are computed by solving the appropriate Fokker-Planck equation. The distribution function should become isotropic for $J \gg J_{lc}$ and vanish at the loss-cone. The steady state solution gives rise to a flow of stars through the loss-cone, which is a consequence of the presence of a mass sink at J_{lc} . This is reflected in the boundary condition that the distribution function vanishes at the loss-cone.

The disruption rate in the diffusive regime is given by

$$\Gamma_d = \int_0^{r_{crit}} \frac{da N_{iso}(a)}{t_r \ln(J_m/J_{lc})} \approx \frac{(r_{crit}/r_a)^{3/2} N_a}{t_r \ln(J_m/J_{lc})}. \quad (14)$$

(e.g. Lightman & Shapiro 1977; Hopman & Alexander 2005).

Here $N(a)da \propto a^{2-\alpha} da$ is the number of stars with semi-major axes in the range $(a, a + da)$. In eq. (14) J_m is to be evaluated at r_{crit} .

Equation (14) is interpreted as a slow diffusion of the angular-momentum of the stars. The time-scale for the angular momentum to change by a factor $\sim J_m = \sqrt{GM_{\bullet}a}$ is of the order of the relaxation time t_r . In a time t_r a significant fraction of the stars within r_{crit} are therefore disrupted by the IMBH. The disruption rate is suppressed by a logarithmic factor which reflects the presence of the loss-cone. This leads to a dilution of stars with small angular momenta in the diffusive regime, as can be seen from the solution of the Fokker-Planck equation (Hopman & Alexander 2005).

For the tidal disruption rate, there is also a contribution from stars for which the change in angular momentum per orbit is larger than J_{lc} (i.e., the regime $a > r_{crit}$). In that case the disruption rate $\Gamma(< a)$ for stars with semi-major axis smaller than a is estimated to be given by the fraction of stars in the loss-cone, divided by the period,

$$\Gamma_d^{kick}(< a) \sim \frac{N(< a)r_t}{aP(a)}. \quad (15)$$

For tidal capture (see below) there is no such contribution, and we do not further consider stars in this “kick” regime here; for a discussion see, e.g., Lightman & Shapiro (1977); Cohn & Kulsrud (1978); Syer & Ulmer (1999); Magorrian & Tremaine (1999).

3.3 Tidal capture

Due to relaxation in angular momentum, any star will eventually be accreted by the IMBH, either because of direct tidal disruption, or due to tidal heating and inspiral. If the number of stars in $(a, a + da)$ which spiral in is given by $N_i(a)da$, and the number of stars which are directly disrupted by $N_d(a)da$, then the probability that the star reaches the IMBH by inspiral is given by

$$S(a) = \frac{N_i(a)}{N_i(a) + N_d(a)} \quad (16)$$

Hopman & Alexander (2005) performed Monte Carlo simulations to show that stars with high energies (small semi-major axes) are unlikely to enter the IMBH without first spiralling in, while stars with low energies (large semi-major axes) are tidally disrupted without experiencing a tidal inspiral phase.

The rate of inspiral is then given by

$$\Gamma_i = \int_0^{\infty} \frac{da N(a) S(a)}{t_r \ln(J_m/J_{lc})}. \quad (17)$$

Here the function $S(a)$ accounts for the fact that capture without premature disruption is improbable for $a > a_c$.

In order for the star to survive, tidal heating should happen at a sub-Eddington rate (see previous section), yielding a minimal value for the pericenter $r_{p,min} \sim 2r_t$. Inspiral without premature scattering is only feasible provided that

$t_0(r_p, a) < t_p(r_p, a)$. As a consequence stars can only spiral in if initially their semi-major axis is smaller than

$$a_{\max} = \left[\frac{3\Delta E_t(r_{p,\min})r_{p,\min}t_r}{2\pi M_* \sqrt{GM_\bullet}} \right]^{2/3}. \quad (18)$$

Note that $t_0 > P$ and thus $a_{\max} < r_{\text{crit}}$, which implies that for tidal capture the relevant regime is the diffusive regime, and that the tidal capture rate is smaller than the rate for tidal disruption, in spite of the fact that tidal heating is efficient for $r_p \lesssim 3r_t$, while tidal disruption happens only for $r_p < r_t$.

The function $S(a)$ may be approximated by a Heaviside step-function $\theta(a - a_c)$, where $a_c \gtrsim a_{\max}$ (Hopman & Alexander 2005). This approximate behaviour is confirmed by our simulations (see §5). The rate at which stars undergo inspiral due to tidal heating and survive is then given by

$$\Gamma_i = \int_0^{a_{\max}} \frac{daN(a)}{t_r \ln(J_m/J_{lc})}, \quad (19)$$

or

$$\Gamma_i \approx \frac{(a_{\max}/r_a)^{3/2} N_a}{t_r \ln(J_m/J_{lc})}. \quad (20)$$

Here the radial stellar distribution function is given by Eq. 8 with $\alpha = 3/2$.

Comparing Eqs. 20 and 14 implies that the rate at which stars in the diffusive regime are tidally disrupted is larger than the tidal capture rate by

$$\frac{\Gamma_d}{\Gamma_i} \approx \left(\frac{r_{\text{crit}}}{a_{\max}} \right)^{3/2}. \quad (21)$$

The actual tidal disruption rate is even higher, because stars with semi-major axes $a > r_{\text{crit}}$ can also be disrupted.

4 DESCRIPTION OF THE N -BODY RUNS

We simulated the evolution of MGG-11 through N -body simulations of star clusters containing $N = 131,072$ (128K) stars using Aarseth's collisional N -body code NBODY4 (Aarseth 1999) on the GRAPE6 computers of Tokyo University (Makino et al. 2003). Following Portegies Zwart et al. (2004), our clusters are initially King models with $W_0 = 9$ and half-mass radius $r_h = 1.3$ pc. The initial mass spectrum of the cluster stars was a Salpeter mass-function between $1.0M_\odot \leq m \leq 100M_\odot$. These cluster models have a projected half-mass radius, mass-to-light ratio and total cluster mass after 12 Myrs that is consistent with the properties of MGG-11 as observed by McCrady et al. (2003). The clusters are also concentrated enough to form IMBHs via runaway merging of stars. Stellar evolution was modelled according to Hurley et al. (2000) and individual runs were calculated for $T = 12$ Myrs. Table 1 gives an overview of the simulations performed.

Stars were merged if their separation became smaller than the sum of their radii and the mass of the merger product was set equal to the sum of the masses of the stars, i.e. we assumed no disruption of stars and no mass loss during a collision. Since typical velocities of stars in our clusters are much smaller than the escape velocities from stellar surfaces, this should be a valid assumption. The mass of tidally

disrupted stars was added to the mass of the central black hole.

In total we performed 12 runs. In six of the runs we used a relation for the radius of the runaway star derived from a fit to the results of Ishii, Ueno & Kato (1999) given by

$$\log \frac{R_*}{R_\odot} = 1.5 \log \frac{M_*}{M_\odot} - 1.85. \quad (22)$$

for stars with $120M_\odot \leq M_* \leq 1000M_\odot$. Radii of more massive stars were set equal to the size of 10^3M_\odot stars. These runs created fairly massive IMBHs with masses between $3000M_\odot < m < 4000M_\odot$. In another set of runs, we used the mass-radius relation found by Bond, Arnett & Carr (1984):

$$\log \frac{R_*}{R_\odot} = 0.47 \log \frac{M_*}{M_\odot} + 0.20. \quad (23)$$

While derived for stars with masses larger than 10^4M_\odot , this relation gives radii in good agreement with the ZAMS radii from Hurley et al. for stars with masses around 10^2M_\odot . These runs lead to runaway stars with masses around $1000 - 2000M_\odot$, roughly equal to the estimated mass of M82 ULX-1. We did not apply stellar mass-loss for the runaway stars and transformed them into IMBHs at $T = 3$ Myrs.

4.1 Implementation of tidal heating into the N -body simulations

We have implemented orbital energy loss by tidal interactions between a star and the IMBH in the N -body simulations using the prescription of Portegies Zwart & Meinen (1993, henceforth PZM). They present fitting formula to the tidal energy loss as a function of the masses, radii and polytropic indices of passing stars. The dimensionless functions $T_l(\eta)$ in eq. (3) for the tidal energy were obtained from a polynomial fit to calculations by Lee & Ostriker (1986) and Ray et al. (1987) for stars of polytropic indices $n = 1.5, 2$ and 3 . PZM found that the $l = 2$ and $l = 3$ terms give a 99% contribution to the dissipated energy and therefore did not take higher harmonics into account.

In our implementation, we assumed that main sequence stars with masses $m < 0.4M_\odot$ and giants have polytropic index $n = 1.5$, while stars with mass $0.4M_\odot < m < 1.25M_\odot$ have polytropic index $n = 2$. More massive main-sequence stars were assumed to have $n = 3$. It was not necessary to apply tidal heating to white dwarfs or neutron stars since these stars were not present in the runs because the studied clusters are too young.

Eq. 3 is only valid if the orbital eccentricity is close to 1. For orbits of smaller eccentricity the amount of tidal heating is smaller since the star feels the influence of the IMBH also at apocenter. In order to reflect this we multiply the heating energy ΔE_t by the eccentricity e of the orbit. In our current implementation, the total angular momentum is conserved and an unperturbed IMBH-star system will always circularise at twice the initial pericenter distance r_{pi} .

Due to the structure of NBODY4, tidal heating had to be included in three different places in the code. In the main integrator, we checked the distance of each particle to its nearest neighbour each time it was advanced in time. This is facilitated by the GRAPE hardware which provides the

Table 1. Details of the performed N -body runs. Shown are the mass-radius relation assumed for the runaway stars (Ishii et al. or Bond et al.), the mass $M_{\bullet i}$ of the IMBH at time of its formation (T=3 Myrs), the mass $M_{\bullet f}$ of the IMBH at the end of the run (T=12 Myrs) and the number N_{Dis} of stars tidally disrupted by the IMBH. Final columns give orbital parameters for tidal heating events: Starting time T_{Insp} of the inspiral, duration of inspiral ΔT_{Insp} until the orbit is circularised, mass M_{\star} and radius R_{\star} of the star at time of inspiral, tidal radius R_t of the star, initial pericentre distance of the orbit $r_{p,i}$, ratio of pericentre distance to the tidal radius of the star $r_{p,i}/r_t$, semi-major axis a and eccentricity e of the initial orbit and semi-major axis $r_{p,f}$ after the orbit circularised.

Run	M-R rel.	$M_{BH i}$ [M_{\odot}]	$M_{BH f}$ [M_{\odot}]	N_{Dis}	T_{Insp} [Myr]	ΔT_{Insp} [yrs]	M_{\star} [M_{\odot}]	R_{\star} [R_{\odot}]	R_t [R_{\odot}]	r_{pi} [R_{\odot}]	r_{pi}/R_t	a [R_{\odot}]	e	r_{pf} [R_{\odot}]
1	IMK99	3572.4	3667.5	29	3.16	$1.1 \cdot 10^2$	6.12	3.0	26.2	26.5	1.01	13375	0.998	53.0
					8.94	$1.2 \cdot 10^5$	1.37	1.4	19.3	58.4	3.03	1408	0.959	90.2
					10.12	$1.7 \cdot 10^3$	2.02	1.6	20.4	21.8	1.07	34149	0.999	58.9
2	IMK99	4076.3	4188.9	27	3.05	$2.5 \cdot 10^2$	1.49	1.4	20.8	35.1	1.69	33410	0.999	42.9
					8.92	$1.9 \cdot 10^2$	1.77	1.5	21.1	36.6	1.73	166379	0.999	38.8
					3.13	$5.7 \cdot 10^3$	64.97	44.4	161.1	383.7	2.38	14695	0.974	728.2
3	IMK99	2786.2	3232.7	31	3.41	$7.5 \cdot 10^3$	50.42	30.5	121.6	169.8	1.40	55688	0.997	336.4
					4.80	$6.7 \cdot 10^3$	25.61	1961.8	10082.9	16172.1	1.60	315615	0.949	20475.5
					6.13	$1.5 \cdot 10^3$	17.64	8.3	48.3	113.7	2.36	22883	0.995	120.3
4	IMK99	3325.3	3783.8	40	10.03	$2.6 \cdot 10^5$	1.35	1.3	18.3	36.2	1.98	76953	0.999	69.2
					3.13	$3.7 \cdot 10^2$	48.84	22.5	96.2	149.1	1.55	100084	0.998	196.9
					3.42	$2.0 \cdot 10^4$	49.75	28.9	124.4	185.5	1.49	31597	0.994	370.9
5	IMK99	3190.3	3464.0	18	3.77	$4.6 \cdot 10^3$	39.68	20.5	95.8	130.2	1.36	21103	0.994	252.4
					10.91	$2.0 \cdot 10^2$	3.01	2.0	22.4	23.8	1.06	25552	0.999	47.4
					3.14	$2.0 \cdot 10^2$	61.72	37.5	144.7	485.1	3.35	20418	0.976	447.8
6	IMK99	3603.7	4230.2	39	3.55	$3.3 \cdot 10^3$	1.43	1.4	19.2	24.6	1.28	117399	0.999	51.0
					5.28	$6.3 \cdot 10^1$	2.32	1.7	20.3	23.1	1.14	43542	0.999	42.9
					7.74	$2.7 \cdot 10^4$	21.60	988.0	5499.1	10847.7	1.97	372902	0.971	14373.1
7	BAC84	1980.7	2597.8	28	11.69	$3.6 \cdot 10^4$	15.69	682.7	4249.3	5530.9	1.30	363884	0.998	8503.8
					3.15	$7.9 \cdot 10^4$	65.53	47.3	185.5	688.0	3.71	9642	0.929	623.5
					3.53	$3.0 \cdot 10^3$	46.70	27.5	122.1	565.4	4.63	215807	0.997	248.5
8	BAC84	2064.6	2383.1	19	3.59	$2.9 \cdot 10^3$	29.15	11.8	61.8	154.7	2.50	133332	0.999	199.1
					4.45	$4.9 \cdot 10^3$	37.05	31.2	152.1	192.8	1.27	82735	0.998	385.4
					4.98	$2.5 \cdot 10^3$	25.41	12.7	70.9	120.8	1.70	49705	0.998	222.3
9	BAC84	1147.2	1579.6	19	8.01	$2.0 \cdot 10^3$	9.86	1489.9	11479.4	14360.4	1.25	655428	0.978	22904.6
					3.04	$1.5 \cdot 10^4$	48.36	25.1	89.1	443.2	4.97	19506	0.977	222.2
					3.84	$6.8 \cdot 10^4$	40.74	42.5	166.0	348.5	2.10	30596	0.989	505.2
10	BAC84	1655.3	2009.4	31	5.79	$6.6 \cdot 10^3$	2.05	1.6	17.7	25.2	1.42	45765	0.999	51.7
					3.04	$3.2 \cdot 10^2$	62.04	34.9	116.0	126.3	1.09	157896	0.999	248.2
					3.40	$1.2 \cdot 10^3$	43.49	20.6	79.7	385.2	4.83	56733	0.993	168.7
11	BAC84	1207.3	1565.3	19	3.42	$2.2 \cdot 10^4$	44.00	27.2	85.2	191.4	2.25	21077	0.991	265.7
					4.11	$3.2 \cdot 10^2$	37.93	32.8	112.7	193.8	1.72	251	0.229	238.1
					4.95	$7.4 \cdot 10^3$	27.91	17.3	67.7	177.1	2.62	27882	0.994	195.4
12	BAC84	1700.8	2287.7	20	6.38	$4.4 \cdot 10^5$	12.45	5.5	28.5	93.0	3.27	33949	0.997	130.2
					11.82	$1.8 \cdot 10^5$	12.81	843.1	4328.9	11232.9	2.59	294365	0.962	12043.5
					3.16	$1.1 \cdot 10^4$	50.05	55.3	185.0	250.7	1.35	70838	0.996	368.1
13	BAC84	1655.3	2009.4	31	4.42	$1.8 \cdot 10^3$	35.02	31.9	121.3	239.7	1.98	22510	0.989	264.7
					4.93	$7.9 \cdot 10^3$	31.89	32.4	128.2	293.7	2.29	3538	0.917	284.5
					5.12	$6.2 \cdot 10^3$	28.84	1738.4	7161.1	22012.6	3.07	190684	0.885	14997.0
14	BAC84	1655.3	2009.4	31	5.83	$1.5 \cdot 10^5$	24.35	15.6	68.5	195.8	2.86	45854	0.996	255.2
					6.33	$2.6 \cdot 10^4$	13.34	5.9	31.9	68.3	2.14	145350	0.999	105.7
					9.90	$8.4 \cdot 10^4$	16.94	15.1	75.8	179.5	2.37	44328	0.996	256.5
15	BAC84	1207.3	1565.3	19	11.13	$1.4 \cdot 10^5$	16.13	708.0	3629.3	5552.3	1.53	80890	0.931	9856.8
					5.36	$7.4 \cdot 10^5$	30.87	27.8	104.3	189.4	1.82	49832	0.996	417.8
					6.00	$6.8 \cdot 10^4$	24.54	1357.5	5524.5	22582.5	4.09	104937	0.785	16732.5
16	BAC84	1700.8	2287.7	20	10.06	$5.1 \cdot 10^2$	16.64	14.1	65.9	81.3	1.23	41275	0.998	139.7
					3.30	$3.2 \cdot 10^2$	27.27	10.5	44.2	92.4	2.09	5641	0.984	90.0
					8.32	$1.2 \cdot 10^4$	11.89	1385.5	8154.8	9569.0	1.17	212502	0.955	16101.8
17	BAC84	1700.8	2287.7	20	10.12	$2.5 \cdot 10^4$	16.99	58.9	309.9	924.1	2.98	49761	0.981	1629.2
					11.37	$1.1 \cdot 10^3$	2.33	1.7	17.9	43.7	2.44	89189	0.999	44.2

index of the nearest neighbour for each particle at almost no extra computational cost. The closest encounter distance was calculated once the relative velocity $v_{rel} = \vec{r}_{ij}\vec{v}_{ij}/|\vec{r}_{ij}|$ between two particles switched sign from negative to positive and we applied tidal heating to all stars that passed within $5r_t$ of a massive black hole by decreasing the kinetic

energy of the combined star-black hole system by an amount ΔE_t . Energy was extracted by changing the velocity and position of the black hole and the star when the system was at pericenter. The energy was changed according to eq. 3 such that the total linear and angular momentum remains constant.

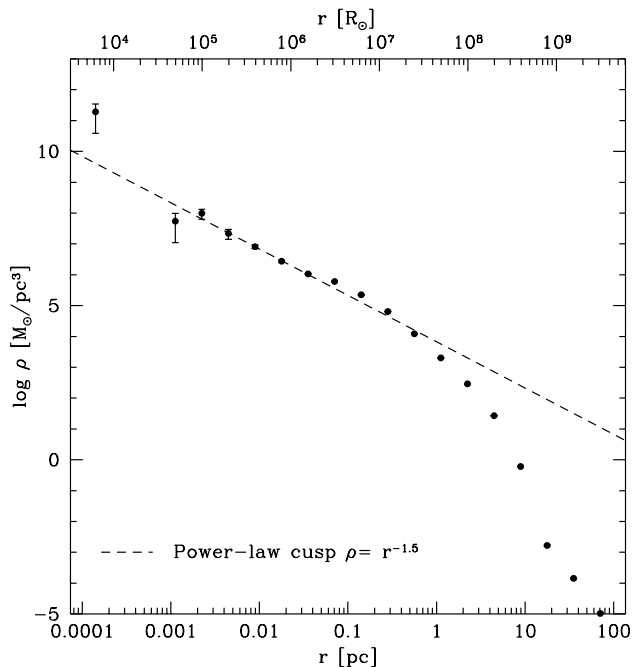


Figure 1. Density profile of run 6 at $T = 3.15$ Myrs, just before an inspiral event happens. Between $10^{-3} \text{ pc} < r < 0.05 \text{ pc}$, the density profile of the cluster follows a power-law cusp with $\alpha = 1.5$. The innermost data point is due to one star which experiences an inspiral at $T = 3.15$ Myrs.

Since in NBODY4 the motion of close particle pairs is followed by KS regularisation (Kustaanheimo & Stiefel 1965), we also had to add tidal heating to the motion of KS binaries. For unperturbed pairs this was done each time their motion was integrated by changing the semi-major axis and eccentricity of the binary according to the accumulated amount of tidal energy. For perturbed binaries, tidal heating was applied after each pericenter passage since at this point the perturbation of the motion of close neighbours is smallest and it is easiest to correct the total energy of the cluster.

Energy dissipation by gravitational radiation was implemented following Peters (1964) formulae in a similar fashion as the implementation of tidal heating.

5 RESULTS

5.1 Central density and mass segregation

We begin by discussing the density profiles of the star clusters after an IMBH has formed in the centre. Fig. 1 depicts the density profile of run 6 from Table 1 at $T = 3.15$ Myrs just before a tidal capture event occurs. The cluster centre is assumed to coincide with the position of the IMBH. It can be seen that the cluster follows a power-law mass density profile $\rho \sim r^{-\alpha}$ with slope $\alpha = 1.50$ inside $r = 0.05 \text{ pc}$. This is close to the value of $\alpha = 1.55$ found by Baumgardt, Makino & Ebisuzaki (2004b) for IMBHs in multi-mass clusters. Inspection of the calculations shows that a cusp is already present by the time the runaway star has collapsed

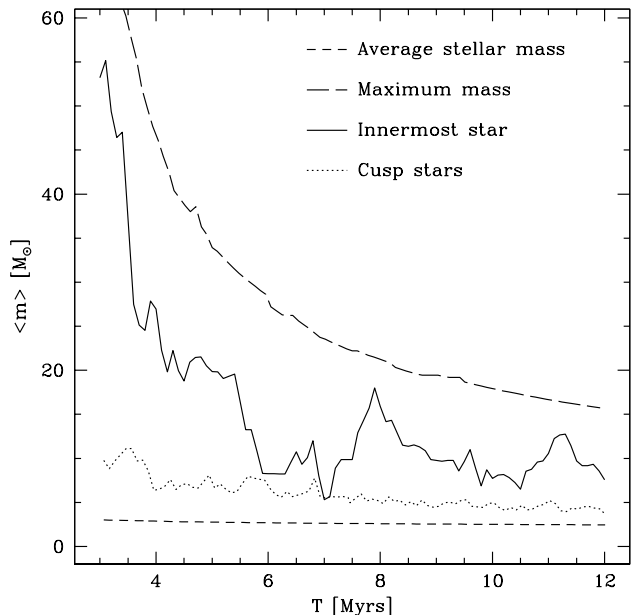


Figure 2. Average and maximum masses of stars in the cluster as a function of time. The masses of all stars decrease as a result of stellar evolution. Due to mass segregation, stars in the cusp around the IMBH are more massive than the average cluster stars and the star closest to the IMBH is always one of the most massive stars in the cluster.

to a black hole (at about 3 Myrs), and as a result already influences the late stages of runaway merging. One reason for the quick formation of cusps is the large initial mass spectrum of our models which reduces the relaxation time. Fig. 1 also justifies our assumptions about the presence of a cusp around the IMBH in §3. Due to the finite number of cluster stars, the central cusp runs out of stars at $r \approx 10^{-3} \text{ pc}$, corresponding to $r = 10^5 R_\odot$. In the present example, one star was pushed to $r = 10^{-4} \text{ pc}$ due to dynamical interactions between the inner cusp stars. This star experiences an inspiral event at $T = 3.15$ Myrs.

Fig. 2 shows average and maximum masses of stars in the cluster and near the IMBH over the course of a simulation. Values shown are averaged over several simulations. Masses of high-mass stars decrease as a result of stellar evolution since stars lose mass in winds and the most massive stars are constantly removed and turned into compact remnants. As a result, the mass of the most massive cluster star, which is near $80 M_\odot$ at $T = 3$ Myrs, drops to $15 M_\odot$ at the end of the simulation. Due to the large number of low-mass stars, the average mass of cluster stars stays nearly constant within the first 10 Myrs at $\langle m \rangle \simeq 3 M_\odot$. Due to mass segregation, the mean mass of stars in the cusp is higher than the mean mass of all cluster stars. Also within the cusp, massive stars sink close to the IMBH so the stars near the IMBH have masses significantly higher than the mean mass. This shows that it is important to take mass segregation into account when determining the inspiral rates.

5.2 Tidal capture

Several trends can be deduced from Table 1:

- Successful inspiral events occur in all runs with on average ~ 4 inspiral events per run during the first 9 Myrs after IMBH formation. Hence there is a high chance that an IMBH in a young star cluster like MGG-11 will undergo a RLOF phase at least once during the lifetime of the cluster.

- Since the masses of stars in the inner cusp are relatively large (see Fig. 2), most inspiral events also involve massive stars. The average mass of captured stars is $\langle m \rangle \approx 25M_{\odot}$, which exceeds the average mass of stars in the cusp. This is caused by the larger cross-section for a tidal interaction with the IMBH of the massive stars.

- In agreement with the theoretical estimates of §3, successful tidal inspiral occurs only for stars in tightly bound orbits around the IMBH with semi-major axis $a < 10^5 R_{\odot}$, the exception being giant stars with much larger radii. This corresponds roughly to the inner end of the cusp. Stars on orbits with larger semi-major also experience tidal interactions with the IMBH (see Fig. 7), but are scattered away by cusp stars before their orbits can circularise.

- Although the cross-section for tidal heating is larger than the cross-section for tidal disruption, it is much more likely to tidally disrupt stars, than to bring a star into a close orbit around the IMBH via tidal heating. Averaged over all runs, we find that the ratio of tidal disruptions to inspirals is $N_d/N_i \approx 7$.

- Successful inspiral events occur predominantly early on in the cluster evolution: Between $5 < T < 12$ Myrs only 24 inspiral events occur compared to 26 events between $3 < T < 5$ Myrs. The decay in the number of tidal inspiral events is mainly caused by the expansion of the cluster, which is driven by mass loss from stellar evolution. In addition, the most massive cluster stars leave the main sequence and increase their radii at $T \approx 3.3$ Myrs, which explains the large number of inspirals around this time involving stars with masses $m > 25M_{\odot}$.

- The final pericenter distances after the orbit circularised, are within a factor of three of the tidal radii since the timescale for tidal circularisation is small only for small r_p/r_t .

As an example for an inspiral event, Fig. 3 depicts the evolution of semi-major axis a and pericenter distance r_p of a captured $m = 17.6 M_{\odot}$ star with time from one of our runs (run 3). The time when tidal heating shrinks the orbit is shown by a solid line. Between 5.3 and 6.1 Myrs the star segregates towards the IMBH as a result of its higher than average mass and the semi-major axis of the orbit shrinks to a few $10^4 R_{\odot}$. Tidal heating occurs at $T = 6.13$ Myrs, when the pericenter distance is scattered to a distance only slightly larger than the tidal radius. During the inspiral the semi-major axis decreases from more than $10^4 R_{\odot}$ to about $120 R_{\odot}$, and the orbit circularises at $r_{pf}/R_t = 2.5$. After the tidal circularisation, the semi-major axis remains unchanged except for perturbations due to passing stars, which increase the eccentricity. Upon each time a small eccentricity is induced, tidal effects will directly start to circularise the orbit again, and so result in a slight decay of the semi-major axis. A strong orbital perturbation causes the star to fill its Roche-lobe at $T \simeq 10.2$ Myr and it is destroyed by the IMBH. Our present N -body code does not allow to treat RLOF phases, a star whose stellar radius expands or whose orbital radius shrinks to the point where the stellar

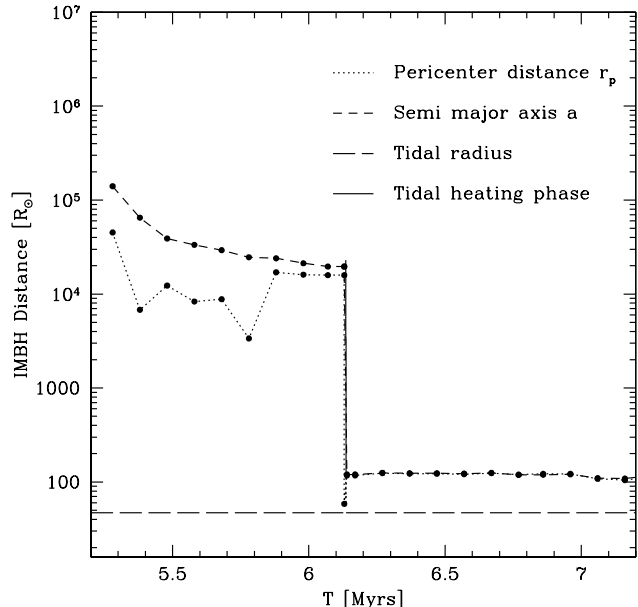


Figure 3. Semi-major axis and pericenter distance of a tidally heated star before and after inspiral due to tidal heating. The main tidal heating event happens at $T = 6.13$ Myrs at which time the star circularises. Later, the semi-major axis changes due to external perturbations while the tidal radius increases as a result of stellar evolution and IMBH growth.

radius exceeds the tidal radius will simply be disrupted. We will present a discussion about the further evolution of such systems based on simple binary-stellar evolution estimates in chapter 5.5.

5.3 Super-Eddington heating rates

The inspiral process may lead to complete tidal circularisation, but also to the destruction of the star. The latter happens if 1) the star passes the black hole’s event horizon or 2) if the rate of energy dissipation in the tidal encounter exceeds the Eddington luminosity. We will now estimate the latter fraction. For each inspiral event we calculated the rate at which energy was pumped into the star due to tidal heating when the eccentricity of the orbit was $e = 0.9$. At this time the amount of energy dissipation per time $\Delta E/P$ reaches a maximum since a and P decrease with e while for smaller eccentricities the stars feel the influence of the black hole also at apocenter and ΔE decreases.

Fig. 4 compares the energy dissipation rates at $e = 0.9$ with the Eddington luminosities of the stars. Super-Eddington heating rates occur in roughly half the cases, but since Fig. 4 shows the maximum heating rates during the inspiral which occur only for a few orbits, cases with $\Delta E_{Insp} > L_{Edd}$ do not necessarily end up in the destruction of the star. Stars might for example lose their outer envelopes and shrink, thereby becoming less susceptible to tidal perturbations, so that the central parts of the stars survive the inspiral. In addition, the extra energy pumped into the star must be larger than the potential energy of the star in order to disrupt it, so the super-Eddington heating rates have to be maintained over many orbits. In order to

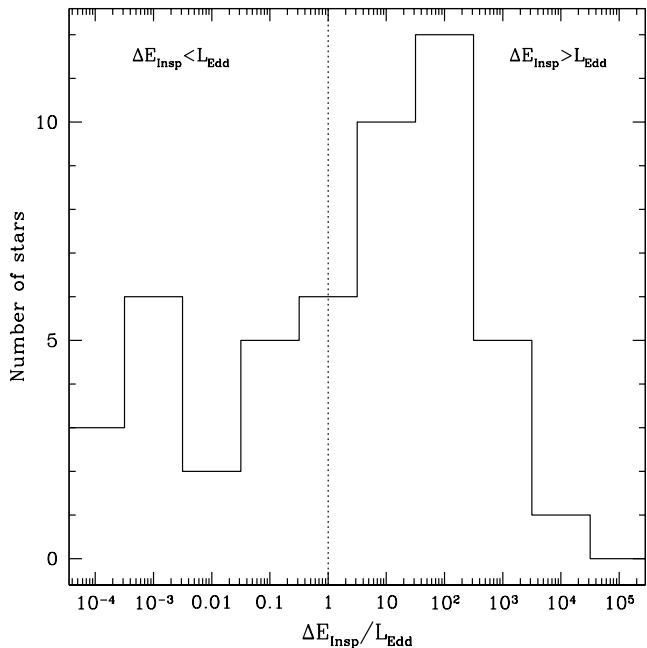


Figure 4. Energy dissipation rates ΔE_{Insp} when the orbital eccentricities have reached $e = 0.9$ compared with the Eddington luminosities L_{Edd} of the stars. Nearly half of all stars experience sub-Eddington heating rates during the inspiral process and survive the inspiral. Moderately super-Eddington stars might also survive the inspiral since the super-Eddington heating rates occur for only short intervals and the extra energy pumped into the star is not sufficient to disperse it completely. If the amount of tidal heating is too large, the stars expand and are tidally disrupted by the IMBH.

answer the question which stars survive the inspiral, more detailed simulations treating the response of the star to the tidal heating would be required. These are beyond the scope of the present paper.

5.4 Comparison with analytical estimates

We compare the numerical results with the analytical estimates from §(3) for the following rather typical example: $M_{\bullet} = 3 \times 10^3 M_{\odot}$, $M_{\star} = 30 M_{\odot}$, $R_{\star} = 10 R_{\odot}$, $t_{rc} = 3$ Myrs, $r_a = 0.05$ pc, $N_a = 300$, and $r_p/r_t = 2.3$. With eqs. (14), (19) and (21) we then find that over a time interval of $T_f = 9$ Myr the number of tidal disruptions is $N_d = \Gamma_d T_f = 8.6$, while the number of tidal captures is smaller by a factor $(r_{\text{crit}}/a_{\text{max}})^{3/2} \simeq 0.08$, $N_i = \Gamma_i T_f \simeq 0.69$, i.e. $N_i/N_d \simeq 0.08$. The maximum distance from which stars can originate is $a_{\text{max}} \simeq 3.4 \times 10^4 R_{\odot}$. By using eq. (13), we also find that the critical radius inside which the loss cone should become empty is $r_{\text{crit}} = 2 \cdot 10^5 R_{\odot}$, slightly larger than the inner end of the cusp.

From our simulations we find that $N_d = 27$, $N_i = 4.1$ and $N_i/N_d = 0.15$. Using only the inspirals which have sub-Eddington heating rates gives $N_i = 1.58$ and $N_i/N_d = 0.06$. Hence the results for the analytical inspiral and disruption rates N_i and N_d are within a factor of 3 to those found in the simulations while the ratio N_i/N_d is correctly predicted.

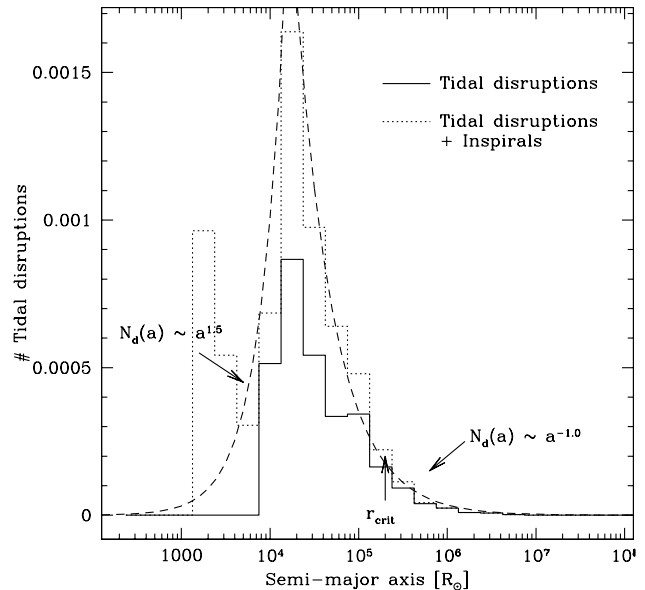


Figure 5. Initial semi-major axis distribution of tidally disrupted stars (solid lines) and combined distribution of tidally disrupted and captured stars (dotted). Shown are differential rates $N(a) = (N(> a) - N(> a + \Delta a))/\Delta a$. The combined distribution has a maximum near the critical radius r_{crit} where the loss-cone becomes empty, in agreement with theoretical predictions (Lightman & Shapiro 1977). The combined distribution can be fitted by two power-laws.

Although tidal disruptions are not the main focus of the present paper, it is interesting to compare them with analytic estimates since the physical processes responsible for inspirals and disruptions are the same. The distribution of semi-major axis of tidally disrupted stars has been calculated by Lightman & Shapiro (1977). They found that the peak in semi-major axis distribution should occur near r_{crit} (see eq. [13]). Inside $r < r_{\text{crit}}$, the loss cone is empty, so stars have to be scattered into the loss cone by two-body relaxation. In this case the number of disrupted stars should be proportional to $N_d(< r) \sim N(< r)/t_r$ which leads to a scaling $N_d(< a) \sim a^{3/2}$ for the number of encounters with semi-major axis smaller than a (see eq. [14]). For the corresponding differential function we find therefore $N_d(a) \sim a^{1/2}$. At larger distance $r > r_{\text{crit}}$ the loss cone is full (“kick” regime); the number of disrupted stars is then given by eq. (15). This leads to a scaling $N_d(> a) \sim a^{-1}$, or, for the differential function $N_d(a) \sim a^{-2}$.

Fig. 5 shows the number of circularised and tidally disrupted stars as a function of the initial semi-major axis. The maximum occurs at $a_{\text{peak}} \simeq 2 \cdot 10^4 R_{\odot}$, somewhat smaller than our analytical estimate for the critical radius r_{crit} .

For radii smaller than a_{peak} , the combined distribution of tidally heated and disrupted stars can be fitted by a relation $N(a) \sim a^{1.5}$. This is somewhat steeper than predicted by Lightman & Shapiro (1977), however the uncertainties in the observed slope are quite large due to the small number of events at small radii. If real, the reason for the discrepancy with Lightman & Shapiro could be the capture of stars by the IMBH followed by three body encounters with other

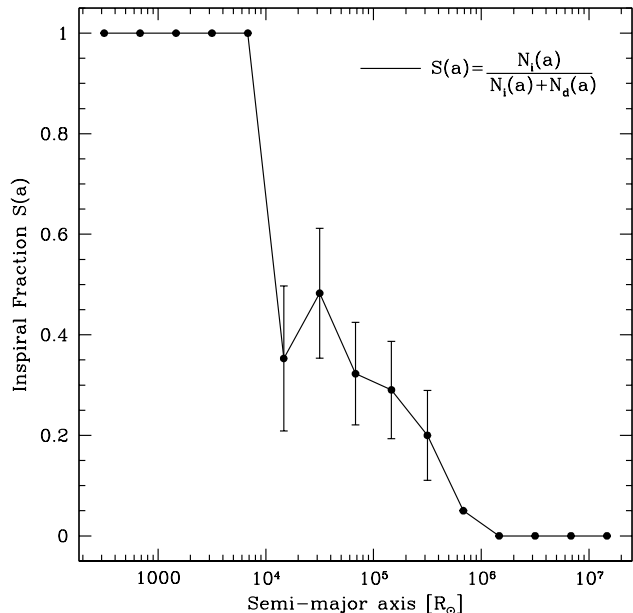


Figure 6. Fraction of tidally captured stars compared to all stars ending in or near the IMBH as a function of the initial semi-major axis a of the stars before tidal capture/disruption (see $S(a)$ in eq. [16]). For small semi-major axis tidal capture dominates while for larger radii tidal disruption becomes the dominant process for feeding the central black hole since stars cannot spiral in any more before being scattered away by other stars.

stars in the cusp. An inspection of the output data shows that these processes contribute considerably to the tidal destruction rate but are not taken into account by our analytic estimates. For radii larger than a_{peak} , we obtain a slower decrease than predicted by Lightman & Shapiro (1977). The reason could be that the stars in the cusp drive the Brownian motion of the IMBH. This influences the determination of the semi-major axis of in-falling stars in case of large semi-major axis.

Hopman & Alexander (2005) found that if stars move slowly through phase space, the number of tidally captured stars should be much larger than the number of tidally disrupted stars for small radii, $N_i(a) \gg N_d(a)$; while for large radii two-body relaxation becomes important and prevents tidal inspiral so $N_d(a) \gg N_i(a)$. In Fig. 6 we compare the number of stars that are tidally heated with all stars that strongly interact with the IMBH. It can be seen that we indeed find the predicted behaviour for $S(a)$.

In §3.3 we demonstrated that the semi-major axis of a stellar orbit has to be smaller than a_{max} in order for the orbit of the star to be successfully circularised. Otherwise the star is scattered away from its orbit due to encounters with other stars. Fig. 7 shows the initial semi-major axis of stars which are tidally heated by the IMBH. Stars for which the inspiral continues all the way until the orbit is circularised are shown by filled circles while stars for which the heating process is terminated since they are either scattered away or experience super-Eddington heating rates during the inspiral process are shown with crosses and triangles respectively.

Tidal capture is only successful if the initial semi-major axis of the star $a \lesssim 2 \cdot 10^5 R_\odot$. The average inspiral distance

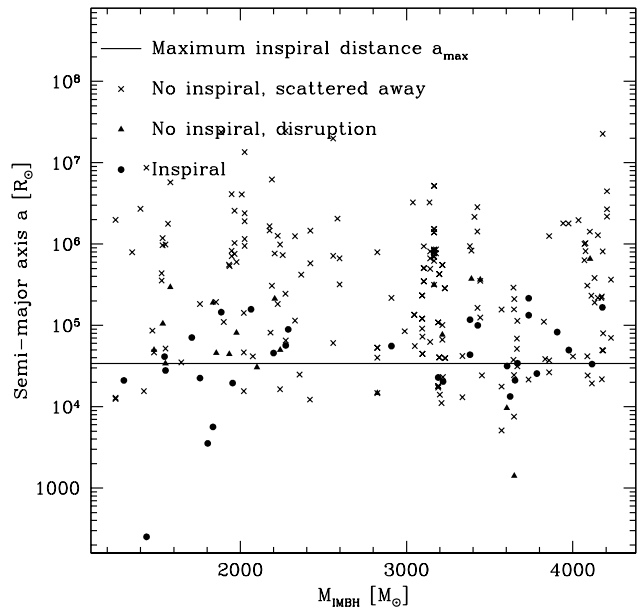


Figure 7. Semi-major axis of tidally circularised stars (dots) compared to stars for which tidal heating does not lead to circularisation (crosses). Successful tidal inspiral is only possible for stars on orbits with small semi-major axis. The threshold between the two cases is in agreement with the prediction of this paper and of Hopman et al. (2004) for the maximum inspiral distance a_{max} .

agrees quite well with the predicted value of a_{max} . Stars circularising due to tidal heating fall into two categories: most of them initially moved on orbits with $e \approx 0.99$ and come from the inner cusp, while few came from relatively low-eccentricity orbits with semi-major axis of a few $1000 R_\odot$. Most of the stars originating from low- a orbits experienced dynamical interactions with previously inspiraled stars.

5.5 Further Evolution of captured Stars

In order to study the mass accretion rate and X-ray luminosity of the IMBHs, we assume that only the innermost stars are close enough to transfer a significant amount of mass to the IMBHs and use the model discussed by K rding, Falcke & Markoff (2002). They assume that X-rays are created in accretion discs and jets and argue that a black hole with a nearby companion is in the hard state if $\dot{M} > \dot{M}_{\text{crit}}$ in which case the disc luminosity is given by $L_X = \epsilon \dot{M} c^2$. At lower accretion rates $L_X = \epsilon \dot{M}^2 c^2 / \dot{M}_{\text{crit}}$. Following their paper, we adopt $\epsilon = 0.1$ and $\dot{M}_{\text{crit}} = 0.1 M_\odot / \text{Myr}$. The mass-loss rates of the donor stars are directly taken from the stellar-evolution routines of Hurley et al. (2000). Stellar winds have typical velocities of about 200 km/sec for LBVs and 1000 km/sec for Wolf-Rayet stars (Paumard et al. 2001), so depending on the orbital separation of the innermost star and the IMBH, gas lost by the star can also escape from the system instead of ending up on the IMBH. A detailed study of gas accretion would require SPH calculations like the ones presented by Cuadra et al. (2005), which are beyond the scope of this paper. In order to account for the loss of gas, we have plotted times when the escape velocity of the star

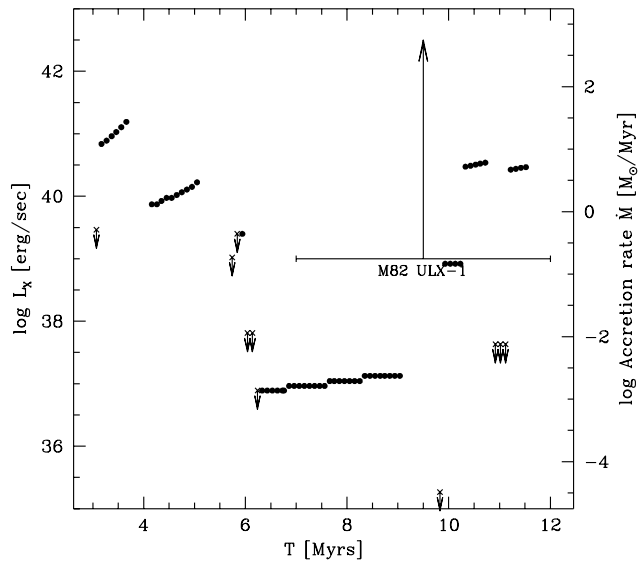


Figure 8. Mass accretion rate and X-ray luminosity of the IMBH of run 10. Crosses denote times when the distance of the star closest to the IMBH is so large that most of the mass lost from the star escapes from the star-IMBH system. Between 3 and 12 Myrs, several close companions to the IMBH formed through tidal heating which transfer mass to the IMBH. For two events, the X-ray luminosity of the IMBH reaches $L_X = 10^{40}$ erg/sec while the stars are on the main-sequence, enough to explain the X-ray luminosity of M82 ULX-1 and also within the right age range of MGG-11.

is smaller than 200 km/sec with crosses. In these cases the values for L_X should be regarded as upper limits.

Figs. 8 and 9 depict the X-ray luminosities of the IMBHs as a function of time for runs 7 and 10. For both clusters, the distance and nature of the innermost star changes rapidly during the simulation as stars near the IMBH are turned into compact remnants by stellar evolution and then scattered out of the cusp by other stars or are tidally disrupted by the IMBH. Run 10 experiences 4 prolonged ULX phases between 3 and 12 Myrs, each time due to massive main-sequence stars brought close to the IMBH as a result of tidal heating. The last two phases are within the right age limits for MGG-11 as determined by McCrady et al. and produce X-ray sources with a luminosity exceeding 10^{40} ergs/sec. Run 10 would therefore be a good candidate to explain the nature of the ULX in M82.

In run 7, three stars experience tidal inspiral between $3 < T < 4$ Myrs and produce ULX sources before the stars are tidally disrupted by the IMBH or turned into compact remnants. At later times, the innermost stars are always too far away from the IMBH for significant mass transfer, hence run 7 is not able to explain the ULX in M82. In total we find that in 10 of the 12 performed runs a ULX source is produced at least once between 3 and 12 Myrs and that 4 out of the 12 runs create an X-ray source brighter than $2 \cdot 10^{39}$ erg/sec within the age range of MGG-11. The average time an X-ray source with a luminosity brighter than 10^{39} erg/sec is present in our runs is 0.96 Myrs, while a source brighter than 10^{40} erg/sec is present for 0.62 Myrs. These values would be lower if tidal destruction of stars with super-Eddington

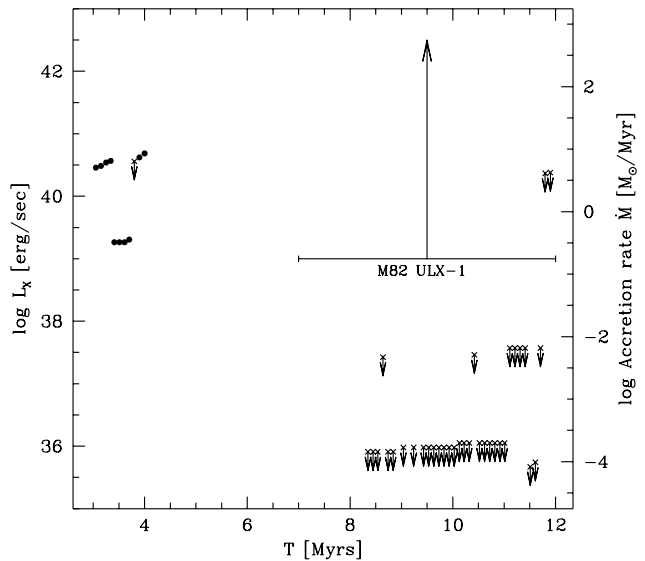


Figure 9. Same as Fig. 8 but now for run 7. This cluster also experiences several inspiral events between 3 and 12 Myrs, but none of them produces an X-ray source which is in the right age range and bright enough to explain M82 ULX-1.

heating rates would be taken into account (see section 5.3), however, at the moment our code does not follow the RLOF phases which would significantly prolong the lifetime of the ULX sources and increase their luminosities. We therefore conclude that an IMBH in a dense star cluster like MGG-11 has a high chance of creating an ULX and that our model can explain the ULX source in M82.

6 CONCLUSIONS

Observations of X-ray sources with luminosities higher than the Eddington luminosity of stellar mass objects provide strong support for the existence of IMBHs. However, the mere existence of an IMBH does not guarantee the existence of ULXs; there has to be a mechanism which accounts for the accretion of gas by the IMBH.

In this paper we confirm the hypothesis that massive ($M_* > 1000 M_\odot$) stars, which may be the progenitors of IMBHs, form naturally in young dense clusters as a result of many collisions between young stars. We assume that the massive star indeed forms an IMBH, and we perform N-body simulations of the interaction between the IMBH and its host cluster, while accounting for tidal encounters between stars and the IMBH. Madhusudhan et al. (2005) found through stellar evolution studies that massive main-sequence stars with masses $M_* > 8 M_\odot$ in orbits of 6 to 30 times the radius of the donor star around an IMBH are necessary to explain ULX sources. Our simulations show that tidal heating of stars in young star clusters will create exactly such systems. We find that, as a result of tidal heating, stars are likely to circularise at distances of a few tidal radii from the IMBH. Once the star has circularised, accretion of stellar gas by the IMBH is sufficient to account for luminosities as high as $L_x \gtrsim 10^{39}$ erg/s. On average, the X-ray luminosities of the circularised stars exceed 10^{39} ergs/sec for

almost 10^6 yrs within the first 12 Myrs in our runs, adding further credibility to the scenario that ULX are IMBHs accreting gas lost from nearby companion stars.

Our conclusions differ from those reached by Blecha et al. (2005). The main reason could be that the IMBHs in our runs are more massive than the ones they considered and they found that higher-mass IMBHs have a higher chance of capturing companions. In addition, they also neglected the effect of mass segregation, whereas in our runs we find that mainly massive stars circularise around the IMBHs.

As we noted in §(5), stars which are tidally captured by an IMBH are typically among the most massive stars in the cluster. The massive star loses much of its energy to other stars by dynamical friction. In a single mass distribution (as is often assumed in an analytical treatment of the problem), diffusion in energy space is very slow (Bahcall & Wolf 1976), but when a spectrum of masses is present, energy loss due to dynamical (non-elastic) interactions with field stars (as opposed to tidal interactions with the IMBH) plays an important role. This further emphasises the importance of mass segregation.

In spite of the fact that some highly simplifying assumptions were made, the final estimate for the rate resulting from our analytical treatment is of the same order of magnitude as what we find from our simulations.

After the donor star leaves the main sequence, it forms a compact remnant. For high-mass donor stars the remnant will be a stellar mass BH and the subsequent evolution of the IMBH-BH binary is driven by the emission of gravitational waves until eventually the binary members merge. Hopman & Portegies Zwart (2005) have shown that the event rate for this is likely to be high enough to be detectable by LISA, in particular if the IMBH mass is larger than $\sim 3 \times 10^3 M_{\odot}$. Observations of gravitational waves from such a binary will give further support for the scenario discussed in this paper. In addition, if IMBHs are formed in star clusters near the centres of galaxies and spiral in due to dynamical friction on the field stars, mergers of the IMBHs with the MBHs at galactic centres would also be important LISA sources (Portegies Zwart et al. 2005).

The mechanism of stellar capture by gravitational wave radiation is similar to that of tidal capture. Mass segregation probably plays a less significant role in the case of the inspiral due to gravitational wave emission by compact remnants when spiralling in to a MBH of $M_{\bullet} > 10^6 M_{\odot}$, because in that case the mass ratio of the field stars is less extreme than is the case for a young dense stellar cluster. The number of compact remnants in galactic centres is not known. Observationally the mass of these objects can be constrained in our Galactic Centre by finding deviations from pure Keplerian orbits, in particular pericenter-shift (Mouawad et al. 2004). Current observational constraints are not conclusive, but this situation will improve with more accurate measurements of the stellar orbits in our Galactic Centre.

In addition to direct disruption and tidal inspiral, we also find a large number of stars that experience one or several strong tidal encounters, but are scattered to wider orbits before they can circularise near the IMBH. As a result of the strong tidal encounters, such tidally heated stars or “tidally scattered” stars are expected to show signs of mixing, large spin and stripping; this may be directly observable in the Galactic centre (Alexander & Livio 2001). We found that on

average there are 45 stars which have one or more interactions of less than $5r_t$ with the MBH and are then scattered away. We expect that this number scales linearly with pericenter distance.

We have assumed that the IMBHs in the clusters formed in a runaway merger of young stars, during a very early stage of cluster evolution. However, other scenarios of IMBH formation have been discussed in the literature. IMBHs may form as remnants of population III stars (e.g. Madau & Rees 2001), or as the merger of stellar mass black holes due to GW emission (Miller & Hamilton 2001). If IMBHs indeed form in these scenarios, and they still reside in stellar clusters, the stars in these clusters will have a much lower maximal mass than in the young clusters we discussed here. If a star is tidally captured, accretion will most likely not lead to high luminosity to account for the most luminous ULXs, although accretion via the subsequent RLOF will lead to a low-luminosity X-ray source.

ACKNOWLEDGEMENTS

We are grateful to Sverre Aarseth for helping us with NBODY4, and to Tal Alexander for interesting discussions. This work is supported by Minerva grant 8484, the Dutch Organization for Scientific Research (NWO under grant # 635.000.001), the Dutch Advanced School for Astronomy (NOVA), and the Royal Netherlands Academy of Arts and Sciences (KNAW). We thank the Sternwarte Bonn and the University of Amsterdam for their hospitality.

REFERENCES

- Aarseth, S. J., 1999, PASP, 111, 1333
- Alexander, T., 1999, ApJ, 520, 137
- Alexander & Livio, 2001, ApJ, 560, L143
- Alexander, T., Hopman, C., 2003, ApJ, 590, L29
- Alexander, T., Morris, M., 2003, ApJ, 590, L25
- Bahcall, J. N., Wolf, R. A., 1976, ApJ, 209, 214
- Bahcall, J. N., Wolf, R. A., 1977, ApJ, 216, 883
- Baumgardt, H., Makino, J., Ebisuzaki, T., 2004a, ApJ, 613, 1133
- Baumgardt, H., Makino, J., Ebisuzaki, T., 2004b, ApJ, 613, 1143
- Blecha, L., et al., 2005, ApJ submitted, astro-ph/0508597
- Bond, J. R., Arnett, W. D., Carr, B. J., 1984, ApJ, 280, 825
- Cohn, H., Kulsrud, R. M. 1978, ApJ, 226, 1087
- Cuadra, J., Nayakshin, S., Springel, V., Di Matteo, T., 2005, MNRAS in press, astro-ph/0502044
- Fiorito, R., Titarchuk, L., 2004, ApJ, 614, L113
- Frank, J., Rees, M. J., 1976, MNRAS, 176, 633
- Freitag, M., 2001, A&A, 375, 711
- Freitag, M., 2001, Class. Quantum Grav., 18, 4033
- Freitag, M., 2003, ApJ, 583, L21
- Freitag, M., Gürkan, M. A., Rasio, F. A., 2005, MNRAS submitted, astro-ph/0503130
- Gutiérrez, C. M., López-Corredoira, M., 2005, ApJ, 622, 89
- Hils, D., Bender, P. L., 1995, ApJ, 445, L7

- Hopman, C., Portegies Zwart, S. F., Alexander, T., 2004, *ApJ*, 604, L101
- Hopman, C., Alexander, T., 2005, *ApJ*, 629, 362
- Hopman, C., & Portegies Zwart, S. F., 2005, *MNRAS*, 363, L56
- Hurley J. R., Pols O. R., Tout C. A., 2000, *MNRAS* 315, 543
- Irwin, J. A., Bregman, J. N., & Athey, A. E., 2004, *ApJ*, 601, L143
- Ishii, M., Ueno, M., Kato, M., 1999, *PASJ*, 51, 417
- Ivanov, P. B., 2002, *MNRAS*, 336, 373, 2002
- Kaaret, P., et al., 2001, *MNRAS* 321, L29
- King A. R., Davies, M. B., Ward, M. J., Fabbiano, G., Elvis, M., 2001, *ApJ*, 552, 109
- Körding, E., Falcke, H., Markoff, S., 2002, *A&A*, 382, L13
- Kochanek, C. S., 1992, *ApJ*, 385, 604
- Kuntz, K. D., Gruendl, R. A., Chu, Y-H, Chen, C.-H., Still, M., Mukai, K., & Mushotzky, R. F., 2005, *ApJ*, 620, L31
- Kustaanheimo, P., Stiefel, E. L., 1965, *J. Reine Angew. Math.*, 218, 204
- Lee, H. M., Ostriker, J. P., 1986, *ApJ*, 310, 176
- Li, Xiang-Dong, *ApJ*, 2004, 616, L119
- Lightman, A. P., Shapiro, S. L., 1977, *ApJ*, 211, 244
- Liu, J-F, Bregman, J. N., & Seitzer, P., 2004, *ApJ*, 602, L249
- Madhusudhan, N., et al., 2005, *ApJ* submitted, astro-ph/0511393
- Makino, J., Fukushige, T., Koga, M., & Namura, K., 2003, *PASJ*, 55, 1163
- McMillan, S. L. W., McDermott, P. N., Taam, R. E. 1987, *ApJ*, 318, 261
- Magorrian, J., Tremaine, S., 1999, *MNRAS*, 309, 447
- Miller, M. C. & Hamilton, D. P., 2001, *MNRAS*, 330, 232
- McCraday, N., Gilbert, A. M., Graham, J. R., 2003, *ApJ*, 596, 240
- Miller, J. M., Fabian, A. C., Miller, M. C., 2004, *ApJ* 614, L117
- Miller, M. C., & Colbert, E. J. M., 2004, *International Journal of Modern Physics D.*, 13, 01
- Miralda-Escudé, J. & Gould, A., 2000, *ApJ*, 545, 847
- Madau, P., & Rees, M. J., 2001, *ApJ*, 551, L27
- Matsumoto, H., et al., 2001, *ApJ*, 547, L25
- Mouawad, N., Eckart, A., Pfalzner, S., Schödel, R., Moutaka, J., Spurzem, R., 2004, *Astronomische Nachrichten* Vol. 326, 2, 83-95
- Peters, P. C., 1964, *Physical Reviews B*, 136, 1224
- Podsiadlowski, Ph., 1996, *MNRAS*, 279, 1104
- Portegies Zwart, S. F., Makino, J., McMillan, S. L. W., & Hut, P., 1999, *A&A*, 348, 117
- Portegies Zwart, S. F., McMillan, S. L. W., 2002 **fillin**
- Portegies Zwart, S. F., Baumgardt, H., Makino, J., McMillan, S. L., Hut, P., 2004, *Nature*, 428, 724
- Portegies Zwart, S. F., Baumgardt, H., McMillan, S. L., Makino, J., Hut, P., Ebisuzaki, t., 2005, *ApJ* submitted, astro-ph/0511397
- Portegies Zwart, S. F., Dewi, J., & Maccarone, T., 2004, *MNRAS*, 355, 413
- Portegies Zwart, S. F., Meinen, A. T., 1993, *A&A*, 280, 174
- Press, W. H., Teukolsky, S. A., *ApJ*, 213, 183
- Preto, M., Merritt, D., Spurzem, R., 2004, *ApJ*, 613, 109
- Rappaport, S. A., Podsiadlowski, P., Pfahl, E., 2005, *MNRAS*, 356, 401
- Ray, A., Kembhavi, A. K., Antia, H. M., 1987, *A&A*, 184, 164
- Rees, M. J., 1988, *Nature*, 333, 523
- Soria, R., Cropper, M., Motch, C., 2004, *Chinese Journal of Ast. & Astrophys.* in press, astro-ph/040913
- Sigurdsson, S., Rees, M. J., 1997, *MNRAS* 284, 318
- Stohmayer, T. E., Mushotzky, R. F., 2003, *ApJ*, 586, 61
- Swartz, D. A., Ghosh, K. K., Tennant, A. F., & Wu, K., 2004, *ApJ*, 154, S519
- Syer, D., Ulmer, A., 1999, *MNRAS*, 306, 35
- Wang, J., Merritt, D., 2004, *ApJ*, 600, 149

This paper has been typeset from a \TeX / \LaTeX file prepared by the author.